

Bayesian Multi-Task Learning MPC for Robotic Mobile Manipulation

Elena Arcari^{*,1}, Maria Vittoria Minniti^{*,2}, Anna Scampicchio¹,
Andrea Carron¹, Farbod Farshidian², Marco Hutter², and Melanie N. Zeilinger¹

Abstract—Mobile manipulation in robotics is challenging due to the need of solving many diverse tasks, such as opening a door or picking-and-placing an object. Typically, a basic first-principles system description of the robot is available, thus motivating the use of model-based controllers. However, the robot dynamics and its interaction with an object are affected by uncertainty, limiting the controller’s performance. To tackle this problem, we propose a Bayesian multi-task learning model that uses trigonometric basis functions to identify the error in the dynamics. In this way, data from different but related tasks can be leveraged to provide a descriptive error model that can be efficiently updated online for new, unseen tasks. We combine this learning scheme with a model predictive controller, and extensively test the effectiveness of the proposed approach, including comparisons with available baseline controllers. We present simulation tests with a ball-balancing robot, and door-opening hardware experiments with a quadrupedal manipulator.

I. INTRODUCTION

In robotics, model uncertainties typically arise when the robot dynamics is not known precisely or when manipulating unknown objects. Uncertainty in model-based control has been treated in many ways. For instance, one can assume that modeling errors in the system dynamics belong to a bounded set, as in robust model predictive control (MPC). Alternatively, prior information in the form of a probability distribution may be leveraged in stochastic MPC, or Reinforcement Learning (RL) methods. While having achieved significant results in challenging non-linear problems, these formulations are designed to remain fixed during operation [1]. Planning for object manipulation, however, requires accurate knowledge of both the kinematic and dynamic parameters of the object. While the former can be identified through vision before executing the task [2], the latter can only be determined by interacting with the object itself. This problem becomes even more challenging for dynamically-stable mobile manipulators, which require precise motion coordination of the mobile base and the arm while maintaining the balance. One way to tackle this is to refine the estimates of model errors using online adaptation or identification procedures as in, e.g., learning-based MPC [3].

This paper addresses online model improvements in the

*The authors contributed equally to this work

¹These authors are with the Institute for Dynamic Systems and Control, ETH Zurich [earcari](mailto:earcari@ascampicco.ethz.ch) | [ascampicco](mailto:ascampicco@ethz.ch) | [carrona](mailto:carrona@ethz.ch) | [mzeilinger](mailto:mzeilinger@ethz.ch)

²These authors are with the Robotic Systems Lab, ETH Zurich [mminniti](mailto:mminniti@robotics.ethz.ch) | [farbodf](mailto:farbodf@robotics.ethz.ch) | [mahutter](mailto:mahutter@robotics.ethz.ch)

This work was supported in part by the Swiss National Science Foundation through the National Centre of Competence in Digital Fabrication (NCCR dfab), and in part by the Swiss National Science Foundation through the National Centre of Competence in Research Robotics (NCCR Robotics).



Fig. 1: The quadrupedal robot ANYmal opening a door. The proposed method learns the model of the manipulated object using data from multiple related tasks (e.g. doors of different masses). When interacting with a new object, the learned model is adapted online using data collected during operation.

context of generating high-performance MPC controllers for robotic mobile manipulation. While the MPC requires an uncertainty representation with low computational overhead, for online learning it is critical to have a descriptive error model that can be efficiently adapted with data available during operation. Therefore, the main challenge is to simultaneously address both issues despite not having necessarily seen the same task before. Robotic manipulation tasks often share a common structure: for example, when manipulating intra-category objects, even though some physical parameters such as damping and stiffness may vary, the model structure remains mostly the same. We leverage this by proposing a Bayesian multi-task, learning-based MPC scheme, where the model error is approximated by means of shared trigonometric basis functions, which are linearly combined with task-specific parameters [4]. The choice of sinusoidal features provides a low-complexity representation of the error dynamics [5], reducing the computational burden of the MPC in evaluating the model and its derivative along the time-horizon. The proposed scheme consists of a training and an online learning phase. In the training phase, we optimize over shared error model hyperparameters using a set of data acquired while performing similar tasks. In the online learning phase, we fix the previously identified basis functions, and fine-tune the error model by adapting the linear parameters using data collected during a new, and potentially unseen, operation.

Contributions: We present a method that combines an adaptive, multi-task learning approach with MPC for robotic mobile manipulation, enabling the proposed scheme to run in real-time on a robot’s onboard computer, while identifying

the model error in the MPC system dynamics. The proposed controller is tested on two mobile manipulators: (i) an underactuated ball-balancing robot (*ballbot*) in the presence of uncertainty in its dynamics, and (ii) a quadrupedal manipulator in a door-opening task with a partially unknown door model (see Fig. 1), building on previous work that attains nominal whole-body loco-manipulation [6], [7]. We present results in simulation and hardware experiments, comparing the proposed approach against other adaptive MPC controllers where the model error is identified via single-task learning and methods that use non-sinusoidal basis functions, e.g. neural networks. We demonstrate that the proposed method outperforms the considered baselines.

Related Work: Multi-task learning, also known as *learning-to-learn* or *meta-learning*, leverages past data in the form of previously observed tasks, to construct an initial prior that can be efficiently used to learn in unseen scenarios. For instance, in [8], the authors propose a multi-robot transfer learning framework that combines \mathcal{L}_1 -adaptive control and iterative learning control. In [9], control-oriented meta-learning is used to identify the non-linear basis functions of the employed adaptive controller. While addressing the issue of efficient online adaptation, these controllers do not exploit the inherent constraint handling and predictive capability of MPC.

In model-free RL, learning from multiple tasks was employed to mitigate data demand, as e.g. in [10], [11], [12], [13]. However, these approaches generally resort to sim-to-real transfer learning [14], and therefore require very accurate models of real-world systems, which are often imprecise or not available.

The combination of single-task learning and model-based control has been successfully applied to multiple robotic platforms, e.g. for fine-tuning nominal models with a learned residual [15], [16], for complex manipulation tasks [17], [18], or to adapt to the presence of unknown loads [19], [20], [21]. However, typically past information from previously observed tasks is not leveraged in a structured manner. This can be enabled, for instance, via multi-task learning, whose combination with model-based approaches has been studied, e.g. in [22], [23]. Multi-task learning methods often make use of non-parametric techniques, as in [24], which exploits latent variable Gaussian processes, or in [25], where deep neural networks are used. While these frameworks can effectively learn complex non-linear dynamics, using them for robotic applications, where stringent computational requirements are imposed by practical hardware limitations, can be challenging. The low-complexity option that we pursue in this work makes use of parametric models, in particular linear combinations of sinusoidal basis functions [4]. Similar ideas are developed in [26], and in [27], [28], which employ Bayesian last-layer neural networks.

II. MULTI-TASK LEARNING FOR MPC

We consider the following non-linear, continuous-time system dynamics

$$\dot{\mathbf{x}} = \mathbf{f}_n(\mathbf{x}, \mathbf{u}) + \mathbf{B}_e \mathbf{e}(\mathbf{x}, \mathbf{u}), \quad (1)$$

where $\mathbf{x}(t) \in \mathcal{X} \subseteq \mathbb{R}^n$, $\mathbf{u}(t) \in \mathcal{U} \subseteq \mathbb{R}^m$ are the state and input of the system. The dynamics of Eq. (1) is modeled as the sum of a *nominal* component \mathbf{f}_n , and an error term \mathbf{e} , which captures the unknown part of the system assumed to lie in the subspace spanned by $\mathbf{B}_e \in \mathbb{R}^{n \times n_e}$. For a robot, this error is typically due to an inaccurate knowledge of the system dynamics parameters, such as masses, CoMs, or inertias of each link, or due to interaction with the external environment. In this paper, the error model is approximated as a linear combination of trigonometric basis functions. The inherent nonlinearity of the resulting parametric model provides a sufficiently rich description, and at the same time a simple structure that can be efficiently adapted online.

In the following, we describe the framework used to learn such parametric approximation. Firstly, the hyperparameters of the sinusoidal features are obtained using a training procedure based on [4]: it consists of an optimization scheme leveraging task data, i.e. noisy error measurements gathered under different operating conditions. Then, we discuss the online learning phase, during which the basis functions are fixed, and the task-specific parameters combining them are adapted online by means of a Kalman filter estimation scheme. Finally, we introduce the optimal control problem (OCP) formulation, and the employed receding horizon strategy generating real-time solutions. A summary of the overall methodology is provided in Fig. 2.

A. Training phase: learning from multiple tasks

We consider the collection of data from M tasks, and assume that we can obtain noisy measurements of the error, resulting in the following measurement model for each element of the error vector $j \in \{1, \dots, n_e\}$:

$$y^{j,m} = e^{j,m}(\mathbf{x}^m, \mathbf{u}^m) + w^{j,m}, \quad m = 1, \dots, M,$$

where $w^{j,m} \sim \mathcal{N}(0, \sigma_w^{j,m})$ is zero-mean Gaussian, task-specific noise. The output $y^{j,m} = \dot{x}^{j,m} - f_n^j(\mathbf{x}^m, \mathbf{u}^m)$ is computed as the difference between the j -th components of the state derivative and the nominal flow-map, evaluated at the *input location* $(\mathbf{x}^m, \mathbf{u}^m)$. In the remainder of the section, we drop the index j for ease of notation and refer to a generic vector element.

1) *Trigonometric basis functions error model:* We store the data collected for each task m into the set $\mathcal{D}^m = \{(\mathbf{x}_i^m, \mathbf{u}_i^m), y_i^m\}_{i=1}^{N_m}$ with cardinality N_m . The considered approximate error model $\hat{e}^m(\cdot, \cdot)$, evaluated at each state-input pair in \mathcal{D}^m , is defined as

$$\hat{e}^m(\mathbf{x}_i^m, \mathbf{u}_i^m) = \boldsymbol{\phi}^m(\mathbf{x}_i^m, \mathbf{u}_i^m)^\top \mathbf{K}^m, \quad i = 1 \dots N_m, \quad (2)$$

where $\mathbf{K}^m \in \mathbb{R}^{2E}$ is a vector of task-specific parameters that linearly combines trigonometric basis functions contained in the vector $\boldsymbol{\phi}^m(\cdot, \cdot) \in \mathbb{R}^{2E}$. The basis function entries are defined for each $i = 1, \dots, N_m$ as

$$[\boldsymbol{\phi}^m(\mathbf{z}_i^m)]_l = \begin{cases} \sin(2\pi\boldsymbol{\omega}_l^\top \mathbf{z}_i^m) & l = 1, \dots, E \\ \cos(2\pi\boldsymbol{\omega}_{l-E}^\top \mathbf{z}_i^m) & l = E + 1, \dots, 2E, \end{cases}$$

where \mathbf{z}_i^m is the vector concatenating the input locations \mathbf{x}_i^m and \mathbf{u}_i^m , and E is the pre-specified number of shared

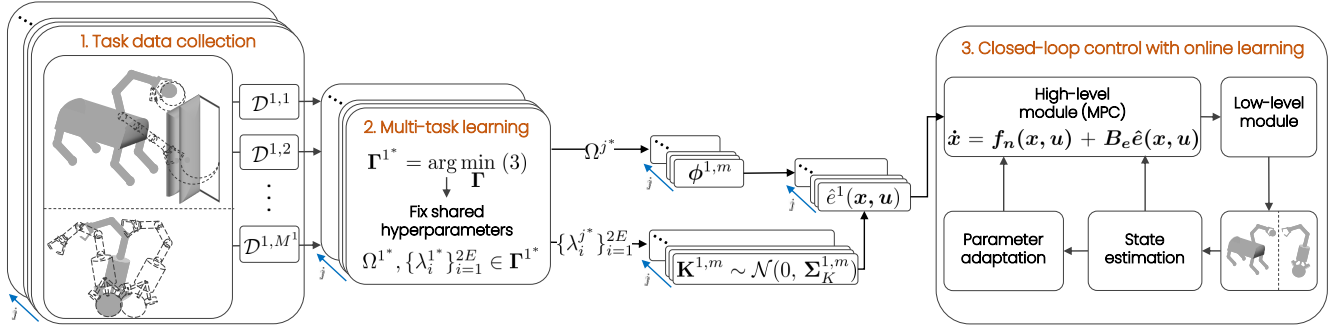


Fig. 2: Overall pipeline of the proposed multi-task learning MPC method for each element $j = 1, \dots, n_e$ of the error vector. For data collection, we let the robot perform M similar tasks under the nominal MPC controller (block 1). This training data is used to optimize a fixed set of shared hyperparameters (block 2). During online execution, the linear parameters $\{\mathbf{K}\}_{j=1}^{n_e}$ are updated via Kalman filtering, and the modeling error is compensated in the MPC (block 3).

frequencies contained in a set $\Omega = \{\omega_1, \dots, \omega_E\}$.

We assume that the vector of coefficients \mathbf{K}^m has a Gaussian prior distribution, such that $\mathbf{K}^m \sim \mathcal{N}(0, \Sigma_K)$, with $\Sigma_K = \text{diag}([\lambda_1, \dots, \lambda_{2E}])$. All hyperparameters $\{\lambda_i\}_{i=1}^{2E}$, $\{\sigma_w^m\}_{m=1}^M$, and Ω are collected in a vector Γ , such that the posterior model for the m -th task is expressed as

$$\hat{e}^m(\mathbf{x}_i^m, \mathbf{u}_i^m)|_{y_i^m, \Gamma} = \phi^m(\mathbf{x}_i^m, \mathbf{u}_i^m)^\top \hat{\mathbf{K}}^m, \quad i = 1 \dots N_m,$$

where $\hat{\mathbf{K}}^m \sim \mathcal{N}(\hat{\mu}_K, \hat{\Sigma}_K)$ is the posterior distribution of \mathbf{K}^m obtained via Gaussian conjugate priors.

Remark 1. Note that this setup can be described as in [4] by considering a shared set of input locations $\bigcup_{m=1}^M \{\mathbf{x}_i^m, \mathbf{u}_i^m\}_{i=1}^{N_m}$. In this case, the noise variance acts as a selector by specifying it as both task and input specific, i.e., for $i = 1, \dots, N_m$:

$$\sigma_{w,i}^m = \begin{cases} \sigma_w^m & \text{if } y_i^m = e^m(\mathbf{x}_i^m, \mathbf{u}_i^m) + w_i^m \text{ exists} \\ \infty & \text{otherwise.} \end{cases}$$

2) *Hyperparameter optimization problem:* We leverage data from $\{\mathcal{D}^m\}_{m=1}^M$ for optimizing the vector of hyperparameters Γ : for each task, a posterior predictive distribution $q^m(\cdot)$ is associated with the approximate model described in Eq. (2), and its “distance” to the true unknown task predictive distribution $p^m(\cdot)$, expressed in terms of the Kullback-Leibler (KL) divergence, is minimized with respect to Γ [4]. In order to express these distributions, the available dataset \mathcal{D}^m is split into two parts, i.e. \mathcal{D}_t^m with cardinality N_t , and \mathcal{D}_v^m with cardinality N_v . The first part is used to compute the posterior distribution of the vector $\hat{\mathbf{K}}^m$, and the second to evaluate the predictive distribution $q^m(\cdot)$ at an input location $(\bar{\mathbf{x}}, \bar{\mathbf{u}}) \in \mathcal{D}_v^m$. Using the metric definition, and approximating the involved expectations with data, the final optimization problem results in

$$\Gamma^* = \arg \min_{\Gamma} \frac{1}{M} \sum_{m=1}^M \frac{1}{N_v} \sum_{(\bar{\mathbf{x}}, \bar{\mathbf{u}}) \in \mathcal{D}_v^m} \log q^m(\bar{y} | (\bar{\mathbf{x}}, \bar{\mathbf{u}}), \mathcal{D}_t^m, \Gamma), \quad (3)$$

where $\Gamma^* = [\Omega^*, \{\lambda_i^*\}_{i=1}^{2E}, \{\sigma_w^{m*}\}_{m=1}^M]$.

B. Online learning phase: task-specific parameter adaptation

Once the trigonometric basis functions’ frequencies Ω^* are inferred during the training phase, these are kept fixed during a new control task, which in general is not one of the M tasks previously observed during training. Furthermore, the vector of parameters \mathbf{K}_0^j is initialized at its optimized prior distribution $\mathcal{N}(0, \Sigma_K^j)$, and is adapted online via Kalman filtering. The parameter process and measurement models are defined as

$$\mathbf{K}_{k+1}^j = \mathbf{K}_k^j + v_k^j, \quad j = 1, \dots, n_e \quad (4a)$$

$$y_k^j = \phi^j(\mathbf{x}_k, \mathbf{u}_k)^\top \mathbf{K}_k^j + w_k^j, \quad j = 1, \dots, n_e \quad (4b)$$

where $v_k^j \sim \mathcal{N}(0, \sigma_Q^j I_{2E})$ is i.i.d. Gaussian process noise, with I_{2E} being the identity matrix of dimension $2E$, and $w_k^j \sim \mathcal{N}(0, \sigma_R^j)$ is i.i.d. Gaussian measurement noise. As specified in Section II-A.1, the measurement noise is considered to be task-specific. For a new, unseen task, one can estimate its variance σ_R^j online via marginal likelihood optimization with an initial batch of data [29], [5] prior to adapting \mathbf{K}^j .

Note that the performance of the Kalman filter in Eq. (4) crucially depends on the knowledge of σ_Q^j , and σ_R^j , and on the accuracy of the error model in Eq. (4b). In particular, if (4b) represents the true model, and under further assumptions on ϕ^j , a tracking error bound for \mathbf{K}_k^j is available [30]. Even if these assumptions are not satisfied, it is possible to compensate for poor knowledge of the error model by manually increasing the filter’s confidence on data, e.g. by increasing σ_Q^j , or by decreasing σ_R^j .

C. MPC formulation

The control problem associated with the system described by Eq. (1) is formulated as the following non-linear OCP:

$$\underset{\mathbf{u}(\cdot)}{\text{minimize}} \quad l_f(\mathbf{x}(T)) + \int_0^T l(\mathbf{x}(t), \mathbf{u}(t), t) dt \quad (5a)$$

$$\text{subject to:} \quad \dot{\mathbf{x}} = \mathbf{f}_n(\mathbf{x}, \mathbf{u}) + \mathbf{B}_e \mathbf{e}(\mathbf{x}, \mathbf{u}) \quad (5b)$$

$$\mathbf{x}(0) = \mathbf{x}_0 \quad (5c)$$

$$\mathbf{g}(\mathbf{x}, \mathbf{u}) = \mathbf{0} \quad (5d)$$

$$\mathbf{h}(\mathbf{x}, \mathbf{u}) \geq \mathbf{0}, \quad (5e)$$

where $l(\cdot, \cdot)$ is the stage cost, $l_f(\cdot)$ is the terminal cost, and T is the time-horizon. Eq. (5c) denotes the initial conditions of the problem, while \mathbf{g} and \mathbf{h} denote state-input equality and inequality constraints, respectively. Model error e is approximated as \hat{e} following the method presented in Sec. II-A, and its parameters $\{\mathbf{K}^j\}_{j=1}^{n_e}$ are adapted online as discussed in Sec. II-B.

In this work, we employ an MPC scheme where, at each time-step, the OCP in (5) is transformed into a finite-dimensional non-linear program (NLP) using a direct multiple-shooting approach [31]. The resulting NLP is solved in a receding horizon fashion using Sequential Quadratic Programming (SQP), for which a detailed description is given in [32]. The MPC problem is solved in a real-time iteration scheme [33], where only one SQP step is performed per MPC update.

III. ROBOTIC MOBILE MANIPULATORS

In this section, we describe how to tailor the OCP in (5) to two application scenarios used to demonstrate the proposed approach: the motion planning problem of a ball-balancing manipulator, and the manipulation planning problem with a quadrupedal manipulator. We refer to Fig. 3 for a schematic representation of the two platforms; in both cases, we use $\{\mathcal{I}\}$ to indicate a fixed, inertial reference frame.

A. Ball-balancing manipulator

The system described in this section is a robot balancing on a ball (*ballbot*) with a 3-DoF arm mounted on top (Fig. 3a) [7]. We model the motion of the mobile base of the robot with $n_b = 5$ degrees of freedom (DoFs), which include the planar position of the ball, denoted as $\mathbf{p}_{B_{xy}} \in \mathbb{R}^2$, and the ZYX angles for the base orientation, denoted as $\boldsymbol{\theta} \in \mathbb{R}^3$. The generalized coordinates of the robot are given by $\mathbf{q} := (\mathbf{p}_{B_{xy}}, \boldsymbol{\theta}, \mathbf{q}_a) \in \mathbb{R}^{n_q}$, where $n_q = n_b + n_a$, $n_a = 3$, and $\mathbf{q}_a \in \mathbb{R}^{n_a}$ are the arm joint angles. We define $\mathbf{x} := (\mathbf{q}, \dot{\mathbf{q}})$, $\mathbf{u} := \boldsymbol{\tau}$, where $\boldsymbol{\tau} \in \mathbb{R}^{3+n_a}$ is given by the torques of the 3 driving wheels and the arm actuated joint torques. The system dynamics of Eq. (1) is then written as

$$\dot{\mathbf{x}} = \left[\mathbf{M}(\mathbf{q})^{-1} [-\mathbf{C}(\mathbf{q}, \dot{\mathbf{q}})\dot{\mathbf{q}} - \mathbf{g}(\mathbf{q}) + \mathbf{S}(\mathbf{q})\mathbf{u}] + \mathbf{e}(\mathbf{q}, \dot{\mathbf{q}}) \right], \quad (6)$$

where $\mathbf{M} \in \mathbb{R}^{n_q \times n_q}$, $\mathbf{C} \in \mathbb{R}^{n_q \times n_q}$, $\mathbf{g} \in \mathbb{R}^{n_q}$, are the nominal mass matrix, Coriolis matrix, vector of gravitational terms and $\mathbf{S} \in \mathbb{R}^{n_q \times (3+n_a)}$ is an actuator-selector matrix.

The vector $\mathbf{e} \in \mathbb{R}^{n_q}$ lumps the uncertainties due to inaccurate knowledge of the robot dynamic parameters (such as masses, CoMs and inertias), which cause the mass matrix, Coriolis matrix and gravitational terms of the real system to deviate from the nominal terms in Eq. (6). We note that, even though uncertainties in the mass matrix can cause the error e to depend on the input \mathbf{u} , in our implementation we neglect this dependence and assume that e is only a function of the state, which allows reducing the dimensionality of the problem. Additionally, to recover the formulation in Eq. (1), the matrix \mathbf{B}_e is chosen such that $n_e = n_q$.

The cost function (5a) used in the MPC formulation is defined as the sum of an end-effector tracking cost and a

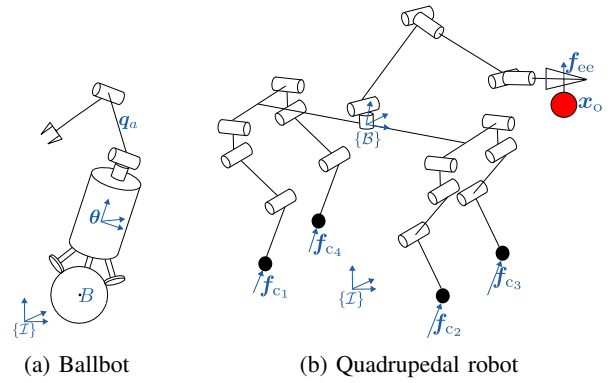


Fig. 3: Schematic representation of a ballbot (Fig. 3a), and of a quadrupedal robot manipulating an object at the end-effector (Fig. 3b). The symbols are defined in Sec. III.

regularization cost to keep the arm joint angles close to a nominal configuration. Joint limits and torque limits (5e) are enforced as soft inequality constraints by means of log-barrier functions [32].

B. Quadrupedal manipulator

Here we describe the planning problem for a quadrupedal robot manipulating an object (Fig. 3b). The nominal MPC strategy was originally presented in [6], where an extensive treatment of the robot model, cost function and constraints is given. Here, we focus on the part of the OCP (5) that concerns the robot interaction with an external object, and extend it to the case where the object dynamics is partially unknown. We define the following vectors:

$$\mathbf{x}_r := \begin{bmatrix} \mathbf{h}_{com} \\ \mathbf{q}_b \\ \mathbf{q}_j \end{bmatrix} \in \mathbb{R}^{12+n_j}, \quad \mathbf{u}_r := \begin{bmatrix} \mathbf{f}_{c1} \\ \vdots \\ \mathbf{f}_{c4} \\ \mathbf{v}_j \end{bmatrix} \in \mathbb{R}^{12+n_j}, \quad (7)$$

where $\mathbf{h}_{com} \in \mathbb{R}^6$ is the robot centroidal momentum, $\mathbf{q}_b \in \mathbb{R}^6$ includes the position and orientation of the base frame \mathcal{B} , and $\mathbf{q}_j \in \mathbb{R}^{n_j}$ is the vector of actuated joints of the legs and the arm. Note that $n_j = 18$, since we consider a robot with 3 DoFs per leg and a 6 DoF arm. In addition, $\mathbf{f}_{c1}, \dots, \mathbf{f}_{c4} \in \mathbb{R}^3$ are the contact forces at the feet, and $\mathbf{v}_j \in \mathbb{R}^{n_j}$ is the vector of actuated joint velocities. We assume that the robot is manipulating an object at the arm end-effector, and define $\mathbf{x}_o = (\mathbf{q}_o, \mathbf{v}_o) \in \mathbb{R}^{2n_o}$ as the object state, where $\mathbf{q}_o, \mathbf{v}_o$ are the object generalized positions and velocities, respectively. The equations of motion of the object can be written as

$$\dot{\mathbf{x}}_o = \left[\mathbf{M}_o^{-1} (-\mathbf{J}_{ee}^T \mathbf{f}_{ee} - \mathbf{b}_o) + \mathbf{e}(\mathbf{q}_o, \mathbf{v}_o) \right], \quad (8)$$

where $\mathbf{M}_o, \mathbf{b}_o, \mathbf{J}_{ee}, \mathbf{f}_{ee}$ are the object mass matrix, the vector of Coriolis, centrifugal, and gravitational terms, the Jacobian of the end-effector contact point, and the force exerted by the object on the robot at the end-effector, respectively. Furthermore, the error term $\mathbf{e} \in \mathbb{R}^{n_o}$ captures all the uncertainties in the object dynamic properties. Crucially, \mathbf{e} is often not known prior to robot-object interaction, and

therefore usually neglected. Letting $\mathbf{x} := (\mathbf{x}_r, \mathbf{x}_o)$, $\mathbf{u} = (\mathbf{u}_r, \mathbf{f}_{ee})$, and choosing \mathbf{B}_e such that $n_e = n_o$, we recover the system dynamics of the MPC problem in Eq. (1).

The stage cost l for the MPC problem in Eq. (5a) is computed as $l = l_r + l_o$. The term l_r penalizes robot-dependent quantities, and l_o is a tracking cost given by

$$l_o = \frac{1}{2}(\mathbf{x}_o - \mathbf{x}_o^{des})^T \mathbf{Q}_o (\mathbf{x}_o - \mathbf{x}_o^{des}) + \frac{1}{2} \mathbf{f}_{ee}^T \mathbf{R}_{ee} \mathbf{f}_{ee}, \quad (9)$$

where \mathbf{x}_o^{des} is a vector of desired object generalized coordinates, and $\mathbf{Q}_o \in \mathbb{R}^{n_o \times n_o}$, $\mathbf{R}_{ee} \in \mathbb{R}^{3 \times 3}$ are weight matrices. Eqs. (5d), (5e) consist of velocity constraints for the swing and stance legs, friction cone constraints for the feet in contact, and joint velocity constraints.

Remark 2. In general, physical limits are implemented as soft constraints in order to preserve feasibility of the MPC problem (5). Under further assumptions [3], stronger guarantees in terms of closed-loop constraint satisfaction in probability can be provided by augmenting the control framework with safety certification mechanisms; these enable corrections to the control input whenever this may lead to constraint violations [34], [35].

IV. RESULTS

The following section is devoted to the empirical evaluation of the proposed approach. First, an object tracking scenario with a simulated quadrupedal manipulator is considered in Sec. IV-A. Further simulations with the ballbot are presented in Sec. IV-B, where the robot needs to follow end-effector targets while keeping balance despite model perturbations. In Sec. IV-C, experimental validation is provided in a door-opening task with a quadrupedal manipulator. A video showcasing the results accompanies this letter ¹.

The following baseline MPC controllers are compared:

- B1) *nominal MPC*: the controller plans with the *nominal* model and neglects the plant-model mismatch [6], [7].
- B2) *ground-truth MPC*: the controller uses the *ground-truth* model of the system.
- B3) *offset compensation*: the error in the MPC dynamics is approximated with an adaptive constant bias, similar to offset-free MPC [36].
- B4) *single-task MPC*: the basis functions hyperparameters are trained on a single dataset. The regression model has the same structure as proposed, and the hyperparameter optimization is based on [5].
- B5) *multi-task MPC*: the proposed method.
- B6) *neural network MPC*: neural network basis functions are considered, similar to [37], and all hyperparameters involved are optimized following Eq. (3).

Note that the approach B2 is a theoretical baseline that can only be implemented in a numerical simulation environment. When testing B3, B4, B5 and B6, the process and measurement noise variances (see Sec. II-B) have the same tuning in each examined scenario. This allows to isolate the effect of the specific type of features (i.e. constant, trigonometric,

TABLE I: Median cost regret w.r.t. ground-truth MPC. Simulation results for the nominal MPC, single-task MPC (using each training dataset), offset compensation, multi-task MPC, and neural network MPC are averaged over 100 noise realizations.

	Task 1	Task 2	Task 3	Task 4
nominal MPC	0.3029	0.2341	0.3730	0.5517
single-task MPC (1)	0.0049	-	-	0.1477
single-task MPC (2)	-	0.1100	-	0.1681
single-task MPC (3)	-	-	0.2412	0.1956
offset compensation	0.0049	0.1013	0.4328	0.1476
multi-task MPC	0.0047	0.0401	0.3313	0.1546
neural network MPC	0.0046	0.1582	3.2508	2.5730

or neural network basis functions). Furthermore, the number of frequencies for B4 and B5 is fixed to $E = 3$, which we observed to work well for all proposed benchmarks. In Eq. (3), we ensure that both training and validation datasets contain measurements of a set-point change.

In all simulations and experiments, we use the OCS2 toolbox [38] for the underlying MPC computations. The hyperparameter optimization for multi-task MPC is carried out with Ipopt [39] within the CasADI [40] environment, while for neural network MPC it is implemented in PyTorch and solved with Adam [41].

A. *Quadruped: object tracking under disturbance*

In this set of simulations, a quadrupedal manipulator needs to move a 1 kg load at the end-effector along specified references. The object state \mathbf{x}_o is given by the position $[x_o, y_o, z_o]$ and velocity $[\dot{x}_o, \dot{y}_o, \dot{z}_o]$ of the load. The equations of motion of the object (Eq. (8)) are artificially perturbed, and we assume that the disturbance on the load is only acting along the world z direction. Despite this modeling choice, the input locations chosen for all baselines consist of the full state \mathbf{x}_o . Each training task is defined by the particular unknown disturbance affecting the trajectory tracking, i.e. task 1 is determined by a constant disturbance $e_1(z_o) = -1.6$, while tasks 2 and 3 by a sinusoid $e_i(z_o) = 3 \sin(2\pi\bar{\omega}_i z_o)$, $i = 2, 3$, with $\bar{\omega}_2 = 2$, and $\bar{\omega}_3 = 6$. Task 4, encountered only during operation, is again induced by a sinusoidal disturbance $e_4(z_o) = 3 \sin(2\pi\bar{\omega}_4 z_o)$ with $\bar{\omega}_4 = 4$.

The proposed multi-task approach is compared against the aforementioned baseline controllers by learning online the error model for each training task (i.e. task 1 to 3), and for the previously unobserved task 4. Simulation results, summarized in Tab. I, are given in terms of median closed-loop cost regret averaged over 100 different noise realizations affecting the error measurement. The cost regret is computed by subtracting the closed-loop cost of the ground-truth MPC from the closed-loop cost of the considered baseline; the closed-loop cost is computed using Eq. (9), i.e. with respect to the terms associated with the object dynamics. Observing Tab. I, for task 1 all methods outperform the nominal MPC and show comparable performance, while for task 2 the proposed multi-task approach outperforms all baselines. The behavior differs between task 3 and task 4: in the first case, the single-task

¹<https://youtu.be/1vlemJKH1aA>

MPC (3), i.e. trained on that particular task, achieves the best performance. However, in terms of dispersion, the multi-task MPC demonstrates superior generalization capabilities in task 4 than its single-task MPC counterparts: despite having lower median, the cost regret values for both single-task MPC (1) and offset compensation belong to the range $[0.1397, 0.3443]$, while the multi-task MPC ranges in $[0.1434, 0.1603]$.

For the neural network MPC, we chose a standard multi-layer perceptron composed of two hidden layers, each with *tanh* activation function, and combined with a last linear 6-dimensional layer to make it comparable with the other sinusoidal-based methods. The closed-loop behavior proved to be sensitive to the choice of the architecture, and particularly to the number of units in the hidden layer, which we fixed to 20. In these simulations, we observed aggressive adaptation along the z axis, which deteriorated the tracking performance in the x and y directions, thereby generating high cost regret (see Tab. I) despite tracking closely the desired set-points in the z direction. Based on these results, neural network basis functions were not further investigated.

Overall, the multi-task MPC shows the most consistent behavior, generally improves performance with respect to the nominal MPC, produces smooth trajectories in all directions, and shows low cost regret for all tasks.

B. Ballbot: perturbing the dynamics model

In the following simulations, the parameters in the ballbot dynamics are perturbed by adding a 1 cm offset along the y axis of the base CoM, a 1 mm offset along all the components of the CoM of the second and last link of the arm, and a 0.355 kg offset to the mass of the last link of the arm. As shown in the accompanying video, this perturbation is enough to cause the closed-loop state under the nominal MPC controller to considerably deviate from the ground-truth state.

The data-collection procedure consists in driving the robot along 7 different trajectories, such that each trajectory, designed to excite a particular degree of freedom, determines a task. The baselines B1-B5 from Sec. IV are tested on a new, unseen trajectory that can be visualized in the accompanying video. For all methods, the error e in Eq. (6) is chosen as a function of the full-state of the robot excluding the xy planar position and the Euler angle θ_z around the world vertical axis. Note that for the single-task MPC, we randomly pick one of the available task datasets for hyperparameter training. The employed MPC time-horizon is 1.5s.

Fig. 4 displays the boxplots of the root-mean-square error (RMSE) between the robot joint positions under each baseline and the ground-truth MPC, collecting data from 100 noise realizations affecting the acceleration measurements. Since the induced error is state-dependent and highly non-linear, the offset compensation setup hardly manages to adapt, and indeed causes the MPC controller to generate joint-space trajectories that lead the arm to singular configurations, as it can be observed in the attached video. On the other hand, the single-task model tends to overfit the training trajectory, showing poor generalization capability. Even though the nominal MPC does not lead the arm to singularity, its

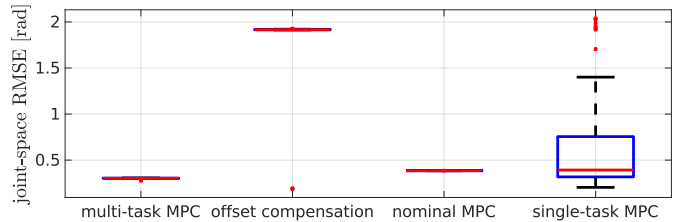


Fig. 4: Boxplot showing the RMSE computed over 100 noise realizations between the ballbot closed-loop joint angles under the ground-truth MPC controller and the baseline controllers.

TABLE II: Median of the final end-effector tracking error, computed over 100 simulation tests with a ballbot under the ground-truth MPC, multi-task MPC and nominal MPC as described in Sec. IV-B.

Method	ground-truth MPC	multi-task MPC	nominal MPC
Final error [m]	0.0167	0.0182	0.0765

performance is affected by the absence of any disturbance identification procedure, and thus also leads to a high end-effector final tracking error (see Tab. II). In conclusion, the closed-loop state under the multi-task MPC controller is the closest to the ground-truth MPC state, thereby improving the end-effector tracking performance.

C. Door-opening hardware experiments

1) *Experimental setup*: The hardware platform employed for the experiments is the ANYmal robot with a 6-DoF arm mounted on top (Fig. 1). As explained in Sec. III-B, the outputs of the MPC computations are feedforward contact forces, generalized positions and velocities, which need to be translated to joint torques. This step is performed by a QP-based whole-body controller running at 400 Hz, which additionally compensates for the full dynamics of the robot [6]. All computations are executed on the robot on-board computer (Intel Core i7- 8850H CPU@4 GHz hexacore processor). The MPC time-horizon is 1 s and the MPC solution is computed at a frequency of 70 Hz.

In the following experiments, the goal of the robot is to pull a door to a desired angle of 70° . The object model in Eq. (8) is $\mathbf{x}_o = [\alpha \ \dot{\alpha}]^T$, where $\alpha, \dot{\alpha}$ are the door-opening angle and its derivative, respectively. The nominal flow-map \mathbf{f}_n assumes that the door has zero stiffness and damping. The measurement of the door dynamics error e relies on estimating the acceleration of the door $\ddot{\alpha}$, which is a challenging task due to the high-impact accelerations arising during trotting [19]. Here, we use a Kalman filter based on a constant acceleration model, which takes measurements of $\alpha, \dot{\alpha}$ as inputs, and computes estimates of $\alpha, \dot{\alpha}, \ddot{\alpha}$. This approach demonstrated to provide sufficiently smooth accelerations for the door-opening task while trotting.

We collect data by executing the door-opening task in the following two scenarios:

- 1) **Added friction**: door pulling experiments with different values of friction between the door and the ground. This

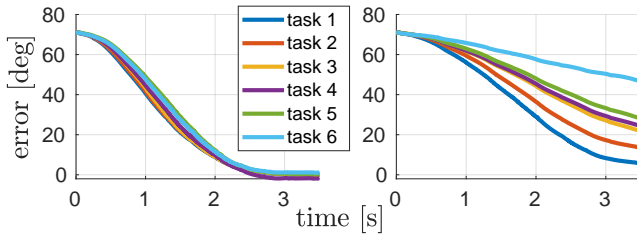


Fig. 5: Tracking error for the door-opening task with added friction under the multi-task MPC (on the left) and nominal MPC (on the right).

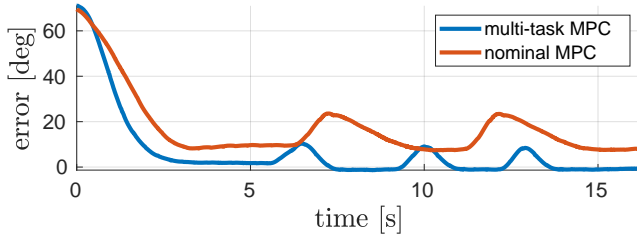


Fig. 6: Tracking error under the multi-task MPC (blue curve) and nominal MPC (red curve) for a door-opening experiment in the presence of human disturbances.

is realized by rigidly attaching a box to the back of the door, and gradually adding weight to it.

- 2) **Human disturbance:** door pulling experiments in the presence of disturbances caused by a person.

The multi-task error model is trained on two datasets from the *Added friction* scenario, and one dataset from the *Human disturbance* scenario. The chosen input locations are the components of the door state (α , $\dot{\alpha}$).

2) *Results:* We perform 7 door-pulling experiments using both the multi-task and the nominal MPC. The testing set consists of 6 tasks from the *Added friction* scenario, including 4 tasks, i.e. friction values, that were not seen at training time, and 1 task from the *Human disturbance* scenario. The door angle tracking error, computed as a difference between the desired and measured door angles, is shown in Fig. 5 and Fig. 6 for the experiments performed in the *Added friction* scenario and *Human disturbance* scenario, respectively.

The tracking error under the nominal MPC controller shows high variability across the different tasks (Fig. 5). This implies that, even if the nominal MPC controller might be well-tuned for a particular door, its performance degrades when the model of the door is perturbed or uncertain. In contrast, the tracking error under the multi-task MPC controller is consistently lower across all tasks. Similarly in Fig. 6, multi-task MPC correctly leads the door back to its desired position, despite repeated human disturbances.

The proposed approach is additionally evaluated against a single-task MPC controller (baseline B4), trained only on one dataset from the *Human disturbance* scenario. Fig. 7 displays the norm of the end-effector force planned by MPC: observing both the plot and the attached video, the behavior in closed-loop is much more aggressive under the single-

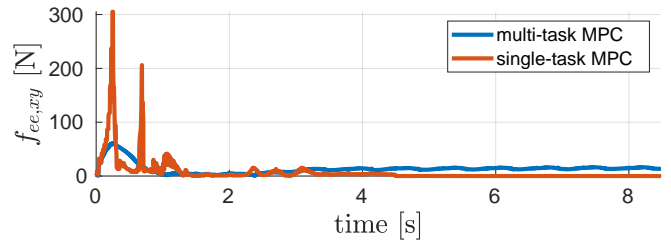


Fig. 7: Norm of the planned end-effector force in a door-opening task with the multi-task MPC (blue curve) and single-task MPC (red curve).

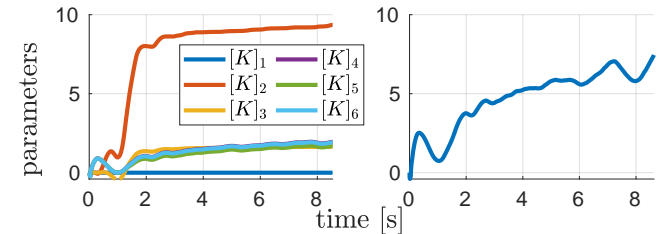


Fig. 8: Task-specific parameters under the multi-task MPC (on the left) and the adaptive bias of the offset compensation-based MPC controller (on the right).

task MPC compared to the multi-task MPC. This is due to oscillations present in the *Human disturbance* dataset that the single-task training tends to overfit, and which do not reflect the natural spectrum of the physical system. In contrast, the multi-task MPC controller results in a smoother behavior. The final experiment, for which no example was included in the training datasets, consists in artificially increasing the spring-stiffness of the door by adding an elastic band between the handle and the door frame. In this scenario, we compare the multi-task MPC controller against its offset compensation counterpart (baseline B3). Fig. 8 displays the task-specific parameters under the two controllers. We observe that under the multi-task MPC, the parameters $[K]_1, \dots, [K]_6$ converge to steady-state values. In contrast, the adaptive constant bias of the offset-compensation MPC diverges. As a result, the robot tends to become unstable, as evident from the oscillations in the right plot of Fig. 8, and the attached video.

V. CONCLUSIONS AND FUTURE WORK

In this work, we presented a Bayesian multi-task, learning-based MPC scheme for robotic manipulation. The core idea is to design a model structure as a linear combination of trigonometric basis functions based on related past experiments, and to efficiently update the model online for high control performance. We evaluated the proposed method in simulation and hardware experiments on a number of robotic scenarios, where the uncertainty in the system dynamics is either due to modeling errors in the robot model or in the manipulated object model. Our results show that the proposed approach is effective when solving control problems in the presence of uncertainties in the system dynamics, consistently outperforming the considered baselines in terms of both identification and tracking performance in closed-loop.

An interesting extension to this work would be to make use of robust or stochastic techniques to provide stability guarantees for the considered model and residual uncertainties, e.g. using ideas from [42]. Another possible research direction could be to relax the assumption of knowing the kinematic parameters, especially when planning for object manipulation. To achieve this, one option could be to use vision sensors to extract the kinematic information of the manipulated object [2], and use that information in the MPC planner.

ACKNOWLEDGMENTS

We thank Daniel Mesham for supporting the implementation in the early stages of this work.

REFERENCES

- [1] L. Hewing, K. P. Wabersich, M. Menner, and M. N. Zeilinger, "Learning-based model predictive control: Toward safe learning in control," *Annual Review of Control, Robotics, and Autonomous Systems*, 2020.
- [2] M. Mittal, D. Hoeller, F. Farshidian, M. Hutter, and A. Garg, "Articulated object interaction in unknown scenes with whole-body mobile manipulation," *arXiv preprint arXiv:2103.10534*, 2021.
- [3] L. Brunke, M. Greeff, A. W. Hall, Z. Yuan, S. Zhou, J. Panerati, and A. P. Schoellig, "Safe learning in robotics: From learning-based control to safe reinforcement learning," *Annual Review of Control, Robotics, and Autonomous Systems*, 2022.
- [4] E. Arcari, A. Scampicchio, A. Carron, and M. N. Zeilinger, "Bayesian multi-task learning using finite-dimensional models: A comparative study," in *IEEE Conference on Decision and Control*. IEEE, 2021.
- [5] M. Lázaro-Gredilla, J. Quiñero-Candela, C. E. Rasmussen, and A. R. Figueiras-Vidal, "Sparse spectrum Gaussian process regression," *The Journal of Machine Learning Research*, 2010.
- [6] J.-P. Sleiman, F. Farshidian, M. V. Minniti, and M. Hutter, "A unified mpc framework for whole-body dynamic locomotion and manipulation," *IEEE Robotics and Automation Letters*, 2021.
- [7] M. V. Minniti, F. Farshidian, R. Grandia, and M. Hutter, "Whole-body mpc for a dynamically stable mobile manipulator," *IEEE Robotics and Automation Letters*, 2019.
- [8] K. Pereida, M. K. Helwa, and A. P. Schoellig, "Data-efficient multirobot, multitask transfer learning for trajectory tracking," *IEEE Robotics and Automation Letters*, 2018.
- [9] S. M. Richards, N. Azizan, J.-J. Slotine, and M. Pavone, "Adaptive-control-oriented meta-learning for nonlinear systems," *Robotics: Science and Systems*, 2021.
- [10] M. Al-Shedivat, T. Bansal, Y. Burda, I. Sutskever, I. Mordatch, and P. Abbeel, "Continuous adaptation via meta-learning in nonstationary and competitive environments," in *International Conference on Learning Representations*, 2018.
- [11] Z. Xu, L. Cao, and X. Chen, "Learning to learn: hierarchical meta-critic networks," *IEEE Access*, 2019.
- [12] X. Song, Y. Yang, K. Choromanski, K. Caluwaerts, W. Gao, C. Finn, and J. Tan, "Rapidly adaptable legged robots via evolutionary meta-learning," in *IEEE/RSJ International Conference on Intelligent Robots and Systems*. IEEE, 2020.
- [13] A. Ghadirzadeh, X. Chen, P. Poklukar, C. Finn, M. Björkman, and D. Kragic, "Bayesian meta-learning for few-shot policy adaptation across robotic platforms," in *IEEE/RSJ International Conference on Intelligent Robots and Systems*. IEEE, 2021.
- [14] W. Yu, J. Tan, Y. Bai, E. Coumans, and S. Ha, "Learning fast adaptation with meta strategy optimization," *IEEE Robotics and Automation Letters*, 2020.
- [15] A. Carron, E. Arcari, M. Wermelinger, L. Hewing, M. Hutter, and M. N. Zeilinger, "Data-driven model predictive control for trajectory tracking with a robotic arm," *IEEE Robotics and Automation Letters*, 2019.
- [16] L. Hewing, J. Kabzan, and M. N. Zeilinger, "Cautious model predictive control using Gaussian process regression," *IEEE Transactions on Control Systems Technology*, 2020.
- [17] I. Lenz, R. A. Knepper, and A. Saxena, "Deepmpc: Learning deep latent features for model predictive control," in *Robotics: Science and Systems*, 2015.
- [18] M. V. Minniti, R. Grandia, K. Föh, F. Farshidian, and M. Hutter, "Model predictive robot-environment interaction control for mobile manipulation tasks," in *2021 IEEE International Conference on Robotics and Automation (ICRA)*. IEEE, 2021, pp. 1651–1657.
- [19] Y. Sun, W. L. Ubellacker, W.-L. Ma, X. Zhang, C. Wang, N. V. Csomay-Shanklin, M. Tomizuka, K. Sreenath, and A. D. Ames, "Online learning of unknown dynamics for model-based controllers in legged locomotion," *IEEE Robotics and Automation Letters*, 2021.
- [20] M. V. Minniti, R. Grandia, F. Farshidian, and M. Hutter, "Adaptive clf-mpc with application to quadrupedal robots," *IEEE Robotics and Automation Letters*, vol. 7, no. 1, pp. 565–572, 2021.
- [21] D. Hanover, P. Foehn, S. Sun, E. Kaufmann, and D. Scaramuzza, "Performance, precision, and payloads: Adaptive nonlinear mpc for quadrotors," *IEEE Robotics and Automation Letters*, 2021.
- [22] L. Zintgraf, K. Shiarlis, M. Igl, S. Schulze, Y. Gal, K. Hofmann, and S. Whiteson, "Varibad: A very good method for Bayes-adaptive deep RL via meta-learning," in *International Conference on Learning Representations*, 2020.
- [23] I. Clavera, A. Nagabandi, S. Liu, R. S. Fearing, P. Abbeel, S. Levine, and C. Finn, "Learning to adapt in dynamic, real-world environments through meta-reinforcement learning," in *International Conference on Learning Representations*, 2019.
- [24] S. Sæmundsson, K. Hofmann, and M. Deisenroth, "Meta reinforcement learning with latent variable Gaussian processes," in *34th Conference on Uncertainty in Artificial Intelligence*, 2018.
- [25] S. Belkhal, R. Li, G. Kahn, R. McAllister, R. Calandra, and S. Levine, "Model-based meta-reinforcement learning for flight with suspended payloads," *IEEE Robotics and Automation Letters*, 2021.
- [26] C. D. McKinnon and A. P. Schoellig, "Meta learning with paired forward and inverse models for efficient receding horizon control," *IEEE Robotics and Automation Letters*, 2021.
- [27] J. Harrison, A. Sharma, R. Calandra, and M. Pavone, "Control adaptation via meta-learning dynamics," in *Workshop on Meta-Learning at NeurIPS*, 2018.
- [28] M. O'Connell, G. Shi, X. Shi, K. Azizzadenesheli, A. Anandkumar, Y. Yue, and S.-J. Chung, "Neural-fly enables rapid learning for agile flight in strong winds," *Science Robotics*, 2022.
- [29] C. E. Rasmussen and C. K. Williams, *Gaussian processes for machine learning*. 2006, 2017.
- [30] L. Guo, L. Xia, and J. Moore, "Tracking randomly varying parameters-analysis of a standard algorithm," 1988.
- [31] H. G. Bock and K.-J. Plitt, "A multiple shooting algorithm for direct solution of optimal control problems," *IFAC Proceedings Volumes*, vol. 17, no. 2, pp. 1603–1608, 1984.
- [32] R. Grandia, F. Jenelten, S. Yang, F. Farshidian, and M. Hutter, "Perceptive locomotion through nonlinear model predictive control," *arXiv preprint arXiv:2208.08373*, 2022.
- [33] M. Diehl, H. G. Bock, and J. P. Schlöder, "A real-time iteration scheme for nonlinear optimization in optimal feedback control," *SIAM Journal on control and optimization*, 2005.
- [34] T. Lew, A. Sharma, J. Harrison, A. Bylard, and M. Pavone, "Safe active dynamics learning and control: A sequential exploration–exploitation framework," *IEEE Transactions on Robotics*, 2022.
- [35] B. Tearle, K. P. Wabersich, A. Carron, and M. N. Zeilinger, "A predictive safety filter for learning-based racing control," *IEEE Robotics and Automation Letters*, 2021.
- [36] G. Pannocchia and J. B. Rawlings, "Disturbance models for offset-free model-predictive control," *AICHE Journal*, 2003.
- [37] J. Harrison, A. Sharma, and M. Pavone, "Meta-learning priors for efficient online Bayesian regression," *International Workshop on the Algorithmic Foundations of Robotics*, 2018.
- [38] "OCS2: An open source library for optimal control of switched systems," [Online]. Available: <https://github.com/leggedrobotics/ocs2>.
- [39] L. T. B. A. Wächter, "On the implementation of a primal-dual interior point filter line search algorithm for large-scale nonlinear programming," *Mathematical Programming*, 2006.
- [40] J. A. E. Andersson, J. Gillis, G. Horn, J. B. Rawlings, and M. Diehl, "CasADi – A software framework for nonlinear optimization and optimal control," *Mathematical Programming Computation*, 2019.
- [41] D. P. Kingma and J. Ba, "Adam: A method for stochastic optimization," in *3rd International Conference on Learning Representations*, 2015.
- [42] J. Köhler, R. Soloperto, M. A. Müller, and F. Allgöwer, "A computationally efficient robust model predictive control framework for uncertain nonlinear systems," *IEEE Transactions on Automatic Control*, 2021.